A role for cytochrome *c* and cytochrome *c* peroxidase in electron shuttling from Erv1

Deepa V Dabir[1,6], Edward P Leverich[1,6], Sung-Kun Kim[2,5], Frederick D Tsai[1], Masakazu Hirasawa[2], David B Knaff[2] and Carla M Koehler[1,3,4,*]

[1]Department of Chemistry and Biochemistry, University of California at Los Angeles, Los Angeles, CA, USA, [2]Department of Chemistry and Biochemistry, Center for Biotechnology and Genomics, Texas Tech University, Lubbock, TX, USA, [3]Molecular Biology Institute, University of California at Los Angeles, Los Angeles, CA, USA, [4]Jonsson Comprehensive Cancer Center, University of California at Los Angeles, Los Angeles, CA, USA and [5]Department of Chemistry and Biochemistry, Baylor University, Waco, TX, USA

Erv1 is a flavin-dependent sulfhydryl oxidase in the mitochondrial intermembrane space (IMS) that functions in the import of cysteine-rich proteins. Redox titrations of recombinant Erv1 showed that it contains three distinct couples with midpoint potentials of −320, −215, and −150 mV. Like all redox-active enzymes, Erv1 requires one or more electron acceptors. We have generated strains with *erv1* conditional alleles and employed biochemical and genetic strategies to facilitate identifying redox pathways involving Erv1. Here, we report that Erv1 forms a 1:1 complex with cytochrome *c* and a reduced Erv1 can transfer electrons directly to the ferric form of the cytochrome. Erv1 also utilized molecular oxygen as an electron acceptor to generate hydrogen peroxide, which is subsequently reduced to water by cytochrome *c* peroxidase (Ccp1). Oxidized Ccp1 was in turn reduced by the Erv1-reduced cytochrome *c*. By coupling these pathways, cytochrome *c* and Ccp1 function efficiently as Erv1-dependent electron acceptors. Thus, we propose that Erv1 utilizes diverse pathways for electron shuttling in the IMS.

Introduction

The mitochondrial intermembrane space (IMS) is conducive to disulfide bond formation (Koehler *et al*, 2006; Wiedemann *et al*, 2006; Herrmann and Kohl, 2007), suggesting that the redox environment is oxidizing, similar to that of the

*Corresponding author. Department of Chemistry and Biochemistry, Molecular Biology Institute, Jonsson Comprehensive Cancer Center, Box 951569, University of California at Los Angeles, Los Angeles, CA 90095, USA. Tel.: +1 310 794 4834; Fax: +1 310 206 4038;
E-mail: koehlerc@chem.ucla.edu
[6]These authors contributed equally to this work

bacterial periplasm (Kadokura *et al*, 2003). Thiol-trapping assays indicated that the small Tim proteins with the twin CX3C motif (Tim8, Tim9, Tim10, and Tim13) form disulfide bonds (Curran *et al*, 2002a, b; Koehler, 2004). Structural and mutational studies confirmed that the small Tim proteins contain juxtapositional disulfide linkages (Allen *et al*, 2003; Lu *et al*, 2004; Webb *et al*, 2006).

Subsequently, a new import pathway was identified for the small Tim proteins and other substrates with a twin CX9C motif (Chacinska *et al*, 2004; Mesecke *et al*, 2005; Rissler *et al*, 2005; Terziyska *et al*, 2005; Gabriel *et al*, 2007). Specifically, Mia40 functions as a tethering component in the IMS by forming a transient disulfide bond with the incoming substrate, trapping the precursor in the IMS. The substrates are released from Mia40 by a mechanism that may involve rearrangement of disulfide bonds. It has been proposed that the sulfhydryl oxidase Erv1 participates in recycling Mia40 by reoxidizing Mia40's cysteine residues (Mesecke *et al*, 2005). Thus, electrons may be transferred from the imported proteins to Erv1 via Mia40. Erv1 also functions in the maturation of cytosolic FeS centers (Lange *et al*, 2001), suggesting its diverse functions in the IMS. Both Mia40 and Erv1 are required for viability (Lisowsky, 1992; Chacinska *et al*, 2004).

Erv1 was first identified by Lisowsky and co-workers (Lisowsky, 1992) and is a member of the flavin-dependent sulfhydryl oxidase family (Coppock and Thorpe, 2006). Erv1 shares homology with Erv2, a protein that functions in the endoplasmic reticulum (Sevier *et al*, 2001), with Quiescin-sulfhydryl oxidases that function in the extracellular matrix (Hoober *et al*, 1996), and with the E10R protein of the pox virus that inserts disulfide linkages into the virion's coat proteins (Senkevich *et al*, 2002). These sulfhydryl oxidases are predicted to use oxygen (O_2) as an electron acceptor for the oxidation of cysteine residues to protein disulfides, generating hydrogen peroxide (H_2O_2) in the process (Coppock and Thorpe, 2006).

Erv1 has three potential redox centers, two pairs of redox-active cysteines (C30–C33 and C130–C133) and a noncovalently bound FAD (Hofhaus *et al*, 2003; Farrell and Thorpe, 2005). The C30–C33 pair is important for the formation of an intermolecular disulfide bond between two Erv1 monomers and is required for *in vivo* function (Lee *et al*, 2000; Hofhaus *et al*, 2003). The C30–C33 pair, however, is not required for sulfhydryl oxidase activity *in vitro*, suggesting that the C30–C33 pair is not required for Erv1 enzymatic activity, but instead serves a structural role. In contrast, the C130–C133 pair, which is positioned near the likely flavin-binding site, is important for the redox activity of Erv1 (Hofhaus *et al*, 2003; Farrell and Thorpe, 2005), as mutagenesis of either cysteine to a serine or alanine abolishes sulfhydryl oxidase activity. Farrell and Thorpe (2005) have estimated an E_m value of −178 mV for the midpoint potential of the flavin in ALR, but were not able to reduce the disulfide near ALR's flavin-binding site (i.e., the disulfide equivalent to C130–C133 in

Erv1), raising the possibility that this putative redox-active cysteine pair in ALR may have a considerably more negative midpoint potential.

Bacteria utilize a wide array of terminal electron acceptors for the oxidative formation of protein disulfide bonds (Bader *et al*, 1999). Erv1 may also display a level of flexibility with regard to electron acceptors, because yeast cells lacking the mitochondrial genome and respiratory pathway still import mitochondrial proteins. In this study, we have used genetic and biochemical approaches to characterize Erv1 and investigate potential pathways in which Erv1 might be oxidized by different terminal electron acceptors. We show that Erv1 forms a complex with cytochrome *c* (cyt *c*) *in organello* and *in vitro*. With *in vitro* assays, we demonstrate that Erv1 shuttles electrons to both O_2 and then cytochrome *c* peroxidase (Ccp1) and oxidized cyt *c*. These studies suggest that, like the prokaryotic disulfide catalytic system, Erv1 utilizes several terminal electron acceptor pathways.

Results

To begin characterization of the electron acceptor pathways utilized by the sulfhydryl oxidase Erv1, we generated temperature-sensitive (ts) mutants using error-prone PCR (Koehler *et al*, 1998). Two strains harboring alleles *erv1-101* and *erv1-12* on centromeric plasmids as well as the *tim9-3* control (Leuenberger *et al*, 2003) grew at 25°C but arrested growth at 37°C on rich glucose (YPD) and ethanol-glycerol (YPEG) media (Figure 1A). We subsequently analyzed the steady-state levels of mitochondrial proteins using α-ketoglutarate dehydrogenase (Kdh) as a loading control (Figure 1B). The abundance of outer membrane markers porin and Tom40 was not affected (data not shown); however, the steady-state

levels of the substrates of the MIA40 pathway (Erv1, Tim9, Tim10, Tim12, and Tim13) and Mia40 were markedly reduced in mitochondria that were shifted to 37°C. In addition, Tim22, Tim23, and Tim54 levels were reduced. The reduction in the TIM22 import components and Tim23 likely results from a decreased import of the small Tim proteins via the MIA import pathway. Interestingly, Ccp1 migrated aberrantly in mitochondria shifted to 37°C, and cyt *c* abundance was not obviously affected at 37°C. Taken together, Erv1 dysfunction affects proteins primarily imported by the MIA40 import pathway and the TIM22 import pathway.

Cyt *c* partners with Erv1 *in organello*

To identify Erv1 partner proteins, we placed 10X-His tags on the C-termini of both Erv1 and Ccp1 and substituted the His-tagged versions on multicopy plasmids for the endogenous genes (Figure 2A and B). The Erv1-His and Ccp1-His strains grew like wild type (WT, data not shown), indicating that the His-tagged proteins were functional. Initial attempts to express Erv1-His from a centromeric plasmid yielded a marked decrease in the Erv1-His protein levels. Therefore, Erv1-His expression from the multicopy plasmid resulted in increased expression of Erv1-His relative to WT mitochondria, whereas cyt *c* and Ccp1 abundance were comparable with that of WT mitochondria (Supplementary Figure 1). Mitochondria were solubilized in 1.0% digitonin (T) and incubated with Ni^{2+} agarose. After washing to remove non-bound proteins (S), the bound proteins (B) were eluted in sample buffer and separated by SDS–PAGE. Immunoblotting analysis showed that cyt *c* and a fraction of the Mia40 co-purified with Erv1-His, whereas Ccp1 did not co-purify. Note that in independent purifications, the fraction of cyt *c* that co-purified with Erv1 varied from approximately 70 to 100% (data not shown),
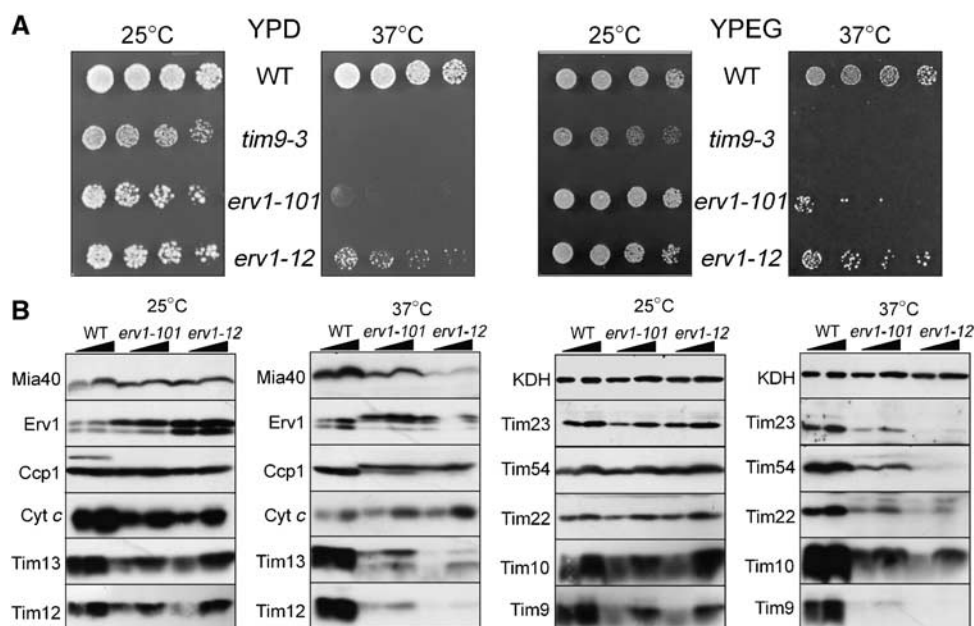

Figure 1 Steady-state levels of IMS proteins are reduced in mitochondria lacking functional Erv1. (**A**) Cells were grown to mid-log phase at 25°C and then serially diluted by a factor of 3 onto rich glucose (YPD) and ethanol-glycerol (YPEG) media before incubation at 25°C and 37°C. Strains included the parent (WT), *tim9-3* mutant, and *erv1* mutants harboring alleles *erv1-101* and *erv1-12*. Plates were photographed after 3–4 days. (**B**) Steady-state levels of mitochondrial proteins (50 and 100 μg) were investigated by immunoblot analyses with antibodies against mitochondrial proteins indicated to the left. Mitochondria were purified from the parent (WT) and *erv1-101* and *erv1-12* strains grown either at the permissive temperature or shifted to the restrictive temperature of 37°C for 7 h.
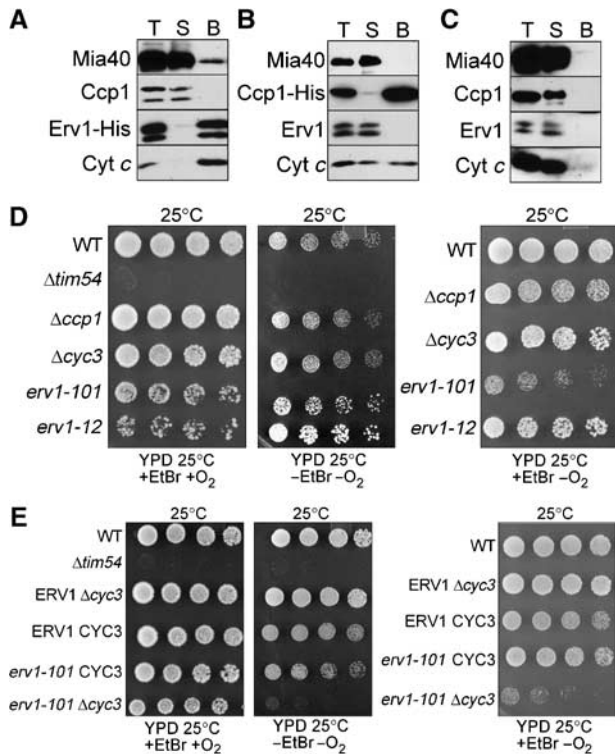
Figure 2 Erv1 and cyt *c* form a complex in the IMS. (**A**) Mitochondria from a strain expressing a C-terminal histidine-tagged Erv1 (Erv1-His) were solubilized at 5 mg/ml in 1% digitonin. As a control, 100 μg of extract was withdrawn (T), and 500 μg lysate was incubated with Ni²⁺-agarose beads. The beads were washed, and bound proteins (**B**) were eluted with SDS–PAGE sample buffer. To assess the effectiveness of binding, 100 μg of the unbound protein fraction (S) was also included. Proteins were analyzed by immunoblotting with polyclonal antibodies against Mia40, Ccp1, Erv1, and cyt *c*. (**B**) Similar to (**A**), except that a C-terminal histidine-tagged Ccp1 was utilized. (**C**) The control reaction in which WT mitochondria have been treated identically. (**D**) Strains (WT, Δ*tim54*, Δ*ccp1*, Δ*cyc3*, and *erv1* mutants, *erv1-101* and *erv1-12*) were serially diluted on YPD medium in the presence and absence of ethidium bromide (EtBr) and incubated in aerobic (+O₂) or anaerobic (−O₂) conditions at 25°C. Plates were photographed after 3–5 days. Petite-negative Δ*tim54* was included as a control. (**E**) A cross between *erv1-101* and Δ*ccp1* that yielded tetratype segregation was analyzed for growth as described in (**D**).

most likely caused by the increased abundance of Erv1-His. With Ccp1-His, a fraction of the cyt *c* but not Erv1 or Mia40 co-eluted. In a control reaction, WT mitochondria were treated identically and the tested proteins showed no affinity for the Ni²⁺ agarose (Figure 2C). Therefore, cyt *c* is a partner protein with both Erv1 and Ccp1, but Ccp1 seemingly does not form a complex with Erv1.

Terminal electron acceptor pathways are required in both aerobic and anaerobic growth conditions, and different pathways are utilized in prokaryotes depending on the oxidative state (Bader *et al*, 1999). First, we tested whether the *erv1* mutants grew under anaerobic conditions and in the presence of ethidium bromide, which induces loss of mitochondrial DNA and respiratory ability (Figure 2D). The *erv1* mutants grew, albeit more slowly, when the mitochondrial genome was absent (+EtBr) under aerobic conditions (+O₂). The *erv1-101* also showed a slower growth rate under anaerobic conditions (−O₂), whether mitochondrial DNA was present or absent (Figure 2D). In contrast, the negative control

Δ*tim54*, which is petite negative, failed to grow under the conditions tested. Because yeast express two different cyt *c* genes (*CYC1* and *CYC7*) under different O₂ concentrations (Burke *et al*, 1997), we used a Δ*cyc3* strain to generate a cyt *c* null strain, as Cyc3 is the heme lyase for assembly of holocytochrome *c* (Dumont *et al*, 1988). The Δ*cyc3* and Δ*ccp1* strains grew under anaerobic and aerobic conditions in the presence and absence of the mitochondrial genome (Figure 2D).

We tested *CYC3* and *ERV1* for synthetic lethality at 25°C (Figure 2E). Tetrad analysis showed that the strain deleted for *cyc3* in the *erv1-101* mutant background was viable in aerobic conditions at 25°C. However, the Δ*cyc3 erv1-101* mutant failed to grow in anaerobic conditions. Thus, *CYC3* and *ERV1* are synthetic lethal in anaerobic conditions, indicating that cyt *c* and Erv1 interact genetically as well as physically.

Erv1 has three different midpoint potentials corresponding to the two redox-active cysteine pairs (C30–C33 and C130–C133) and the FAD moiety

Previous studies have suggested that C30–C33 plays a structural role in the formation of Erv1 dimers, whereas the C130–C133 pair has sulfhydryl oxidase activity and is situated near the FAD (Lee *et al*, 2000; Hofhaus *et al*, 2003). We measured the disulfide/dithiol redox properties of Erv1 at pH 7.0 using GSH/oxidized glutathione (GSSG) redox buffers to poise samples at defined redox potentials (E_h) values ranging from −100 to −240 mV and reduced dithiothreitol (DTT)/oxidized (DTT$_{ox}$) redox buffers to poise samples at E_h values ranging from −220 to −380 mV (Figure 3; Krimm *et al*, 1998; Hirasawa *et al*, 1999). Recombinant Erv1 was incubated in the indicated redox potential buffer and then treated with mBBr to form fluorescent covalent adducts of Erv1 thiols (mBBr does not react with disulfides). The titration results were independent of the redox equilibration time, over the range from 1.5 to 3.5 h, and were also independent of the concentration of the redox buffer, over the range from 1 to 5 mM, indicating the likelihood of good redox equilibration between Erv1 and the ambient potential imposed by the redox buffers. Additional support for the establishment of good redox equilibration during these titrations comes from the fact that all of the titrations gave excellent fits to the Nernst equation for a two-electron redox couple. Figure 3A shows the results of a typical titration and reveals the presence of two two-electron components. The average values (based on three titrations) for the redox midpoint potentials (E_m) of the two components are −330 and −150 mV, respectively (the use of the average deviation as an approximate measure of the experimental uncertainty suggests that the experimental uncertainty does not exceed ± 10 mV). The E_m value and the $n = 2$ character of the titration curve, as well as the known specificity of mBBr for chemical modification of thiols (Krimm *et al*, 1998; Hirasawa *et al*, 1999), indicate that the redox titration results are most readily interpreted in terms of the presence of two separate disulfide/dithiol redox couples in Erv1.

Added support for the notion of two separate thiol-based redox couples comes from DTNB assays of the thiol content of Erv1 samples poised at defined redox potentials (See Table I). In particular, the difference in thiol content of Erv1 samples poised at a potential where the $E_m = −150$ mV transition would be either completely reduced or completely
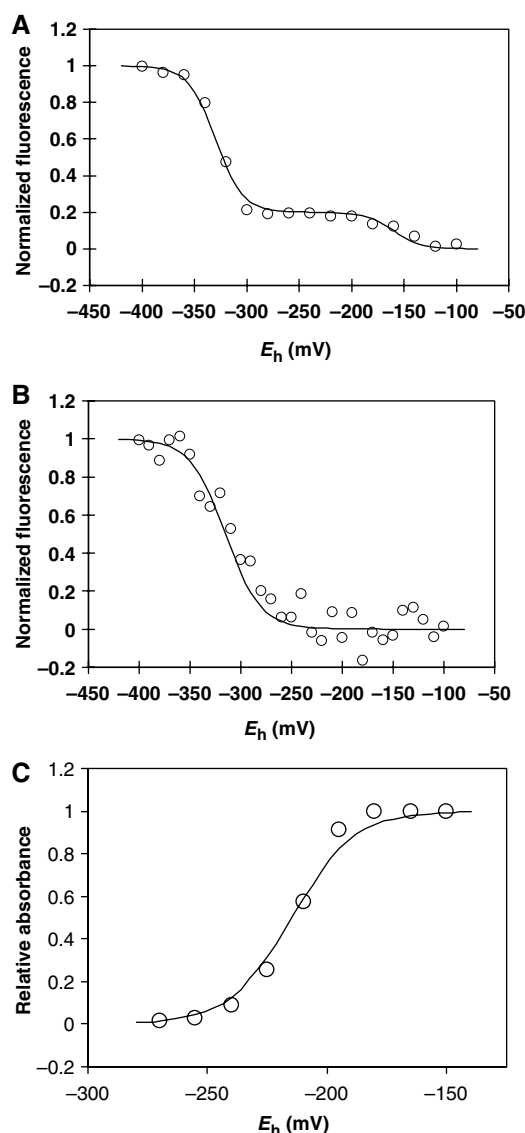
Figure 3 Oxidation–reduction titrations of Erv1 reveal three midpoint redox potentials. (**A, B**) Redox titrations of dithiol/disulfide couples in Erv1 were carried out using DTT or glutathione redox buffers. Redox equilibration was performed for 2 h at pH 7.0 with total redox buffer concentrations of 2.0 mM. Data in all titrations were fitted to the Nernst equation for a two-electron carrier. In (A), the titration was tested using the mBBr method. The best fit to the mBBr fluorescence magnitude versus E_h value was obtained for the presence of two separate ($n=2$) components, with E_m values of -330 and -150 mV, respectively. In (B), the titration was performed using intrinsic tryptophan fluorescence to monitor the redox state of Erv1. The best fit to the data was for a single ($n=2$) component with $E_m = -315$ mV. (**C**) The redox midpoint potential of the flavin group was determined by electrochemical titration of Erv1 ($10.0\,\mu$M) at 10°C in 50 mM KPO$_4$, pH 7.0, in the presence of $10\,\mu$M benzyl viologen, $10\,\mu$M anthraquinone-2-sulfonate, and $10\,\mu$M 2-hydroxy-1,4-napthoquinone as redox mediators. The difference in absorbance at 465 nm minus that at 550 nm was used to monitor the extent of FAD reduction. The value of this absorbance difference for the fully oxidized FAD was set as 1.0 and the value for the fully reduced FAD was set at 0.0, to define the relative absorbance difference scale. The open circles represent the measured relative absorbance and the solid line is the computer best fit of these data to the Nernst Equation for a two-electron redox couple with $E_m = -215$ mV. Representative individual spectra taken at different defined E_h values are shown in Supplementary Figure 3.

Table I DNTB addition assay to Erv1 equilibrated at different E_h values (based on calculated E_m potentials)

Redox potential at which Erv1 is equilibrated	Mole of free thiol per mole of Erv1
Fully reduced, denatured	6.0 ± 0.1
Fully reduced (-400 mV)	3.0 ± 0.1
Half reduced (-240 mV)	2.1 ± 0.2
Fully oxidized (-90 mV)	0.1 ± 0.1

oxidized is 2.0 ± 0.3 mol of thiol per mol of Erv1, exactly what would be predicted for the reduction of one intramolecular disulfide per Erv1 monomer. Similarly, the difference in thiol contents of Erv1 samples poised at potential where the $E_m = -320$ mV transition would be either completely reduced or completely oxidized is 0.9 ± 0.3 mol of thiol per mol of Erv1, exactly what would be predicted for the reduction of one intermolecular disulfide between two Erv1 monomers.

An attempt was made to confirm the assignment, based on DTNB thiol assays of samples poised at defined E_h values, of the $E_m = -330$ mV to an intermolecular disulfide formed between two Erv1 monomers, using non-reducing SDS–PAGE gels of Erv1 samples that had been poised at defined E_h values centered around -330 mV before SDS–PAGE analysis. The amount of dimer increases as the E_h is increased over the range from -380 to -220 mV (Supplementary Figure 2), consistent with an E_m value of approximately -330 mV for an intermolecular disulfide. Figure 3B shows the results of a redox titration, achieved under conditions identical to those of Figure 3A (except that mBBr was not added), but with tryptophan fluorescence used to monitor redox-dependent changes in Erv1. The data are most readily interpreted in terms of a two-electron redox couple, with $E_m = -315 \pm 10$ mV at pH 7.0, in which the microenvironment of at least one Erv1 tryptophan residue differs in the oxidized and reduced forms of the protein. The fact that the E_m value of the two-electron couple detected in tryptophan fluorescence is indistinguishable, within the combined experimental uncertainties of the measurements, from the E_m value of the more negative couple seen in the mBBr titrations, leads us to conclude that it is the monomer/dimer transition that alters the microenvironment of at least one Erv1 tryptophan.

Flavin analysis of Erv1 indicated the presence of 1.0 ± 0.1 mole of FAD per mole of recombinant Erv1 (no evidence was found for any FMN in the protein). Figure 3C shows the results of a typical titration of the FAD group of Erv1 at pH 7.0, using the absorbance in the visible region to monitor the oxidation state of FAD. The data showed an excellent fit to the Nernst equation for a single $n=2$ component with an E_m value of -215 mV. Representative spectra generated during the potentiometric titration of the flavin group are included (Supplementary Figure 3). The absence of well-defined isosbestic points in these spectra arises from a slow drift in the instrument baseline during the approximately 2 h required for the full titration. Under the conditions employed, no red anionic or neutral blue flavin semiquinone could be detected, in contrast to the results reported for ALR (Farrell and Thorpe, 2005). It should also be pointed out that while the flavin in ALR has been suggested to have a more positive redox potential than the disulfide/dithiol centers present in ALR (Farrell and Thorpe, 2005), this is not the case for Erv1

where the FAD has an E_m value that is significantly more negative than that of the $E_m = -150\,mV$ intramolecular disulfide.

Erv1 and cyt c interact in a 1:1 complex and Erv1 can directly reduce cyt c

Farrell and Thorpe (2005) have previously suggested that cyt *c* is the physiological oxidant of Erv1. In Figure 2A, we demonstrated that cyt *c* partners with Erv1 *in vivo*. To further probe the stoichiometry of the Erv1:cyt *c* complex, we examined the interactions of our characterized recombinant Erv1 and yeast cyt *c*, using a spectral perturbation technique to monitor protein–protein interactions. This technique has been used to characterize a large number of protein complexes, including the one formed between cyt *c* and Ccp1 (Erman and Vitello, 2002). The solid line in Figure 4A shows the difference spectrum arising from the interaction of Erv1 with cyt *c* in low ionic strength buffer (i.e., it represents the spectrum of a 1:1 mixture of the two proteins from which has been subtracted the sum of the spectra of the two separate proteins). This difference spectrum was not observed if either BSA or Ccp1 replaced cyt *c*, suggesting that the difference spectrum of Figure 4A does not arise from some nonspecific artifact. Figure 4A also shows (see the dashed line) that no spectral perturbations are observed at high ionic strength (solid NaCl was added to the sample used for the low ionic strength spectrum to yield an approximate concentration of 250 mM and the spectrum was re-recorded). The simplest explanation for this observation is that electrostatic forces, which weaken at high ionic strength, make an important contribution to stabilizing the Erv1:cyt *c* complex. Figure 4B shows the results of an experiment, carried out at low ionic strength, in which the magnitude of spectral changes arising from complex formation were plotted against varying concentrations of cyt *c* at a fixed concentration of Erv1. The data give a good fit to the theoretical curve for the presence of a 1:1 Erv1:cyt *c* complex of very high affinity (computer simulations suggest that the K_d for complex formation under these conditions is probably $\leqslant 100\,nM$). As protein–protein complex formation can alter the E_m value of protein prosthetic groups (Ondrias *et al*, 1985), the FAD group of Erv1 and the heme of cyt *c* were titrated in a 1:1 mixture of the proteins at the low ionic strength that favors complex formation between the proteins. The E_m value of the Erv1 FAD was unaffected by the presence of cyt *c* and the E_m value of cyt *c* was found to be $+250\,mV$, regardless of whether Erv1 was present or absent (data not shown). The value obtained in the absence of Erv1 is in good agreement with the published literature (Wallace, 1984).

That Erv1 and cyt *c* form a complex suggests that Erv1 might shuttle electrons directly to cyt *c*. This possibility was tested directly, under anaerobic conditions, by observing changes in absorbance at 550 nm that arise from reduction of the cyt *c* heme when DTT-reduced Erv1 is added to ferric cyt *c* (Figure 4C). Erv1, at the concentration used in these experiments, does not contribute significantly to the absorbance at this wavelength. As shown in Figure 4C, the addition of reduced Erv1 indeed cause rapid reduction of cyt *c*, denoted by the marked increase in absorbance after Erv1 addition. In control experiments, in which DTT alone was added to cyt *c* in the absence of Erv1, a much slower rate of heme reduction was observed, indicating that DTT is a
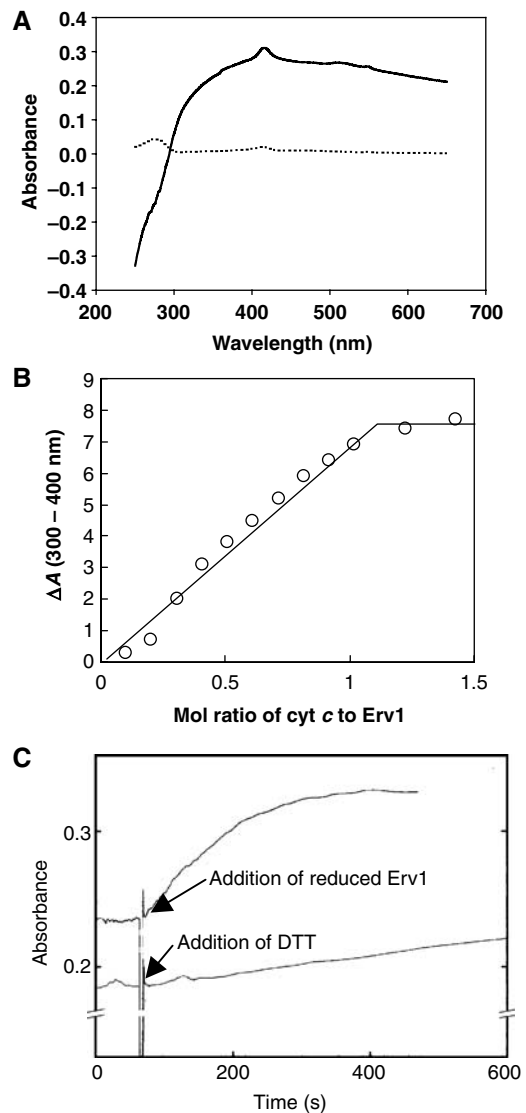

Figure 4 Erv1 and cyt *c* form a 1:1 complex, in which Erv1 reduces cyt *c* directly. (**A**) A representative run showing the difference spectra resulting from complex formation between a 1:1 M ratio of Erv1 and cyt *c*. The solid line represents the spectrum arising from the complex under low ionic buffer (10 mM KPO$_4$, pH 7.0); dashed line represents the spectrum from the complex in high ionic buffer (250 mM NaCl, pH 7.0). (**B**) Binding isotherms for complex formation at pH 7.0 between Erv1 and cyt *c* were monitored by changes in the UV/visible region of the absorbance spectrum. Increasing concentrations of cyt *c* as indicated were added to Erv1. The spectrum was not perturbed further when cyt *c* was added at an Erv1:cyt *c* molar ratio of greater than 1:1, suggesting a 1:1 complex. (**C**) The reduction of cyt *c* by Erv1 was measured at 550 nm as a function of time. The concentration of cyt *c* was fixed at 10 μM; Erv1 and DTT concentrations were 2.3 μM and 0.4 mM, respectively.

kinetically poor reductant for cyt *c* and confirming that Erv1 can reduce the heme of cyt *c* directly *in vitro*.

Ccp1 and cyt c compete with O₂ in Erv1-mediated oxidation of DTT

Ccp1 serves as a general catalyst to remove H_2O_2 formed in mitochondria during aerobic metabolism (Boveris, 1976). However, despite extensive *in vitro* characterization of Ccp1 (Erman and Vitello, 2002), few studies have clarified its specific physiological role in yeast. We tested *CCP1* and
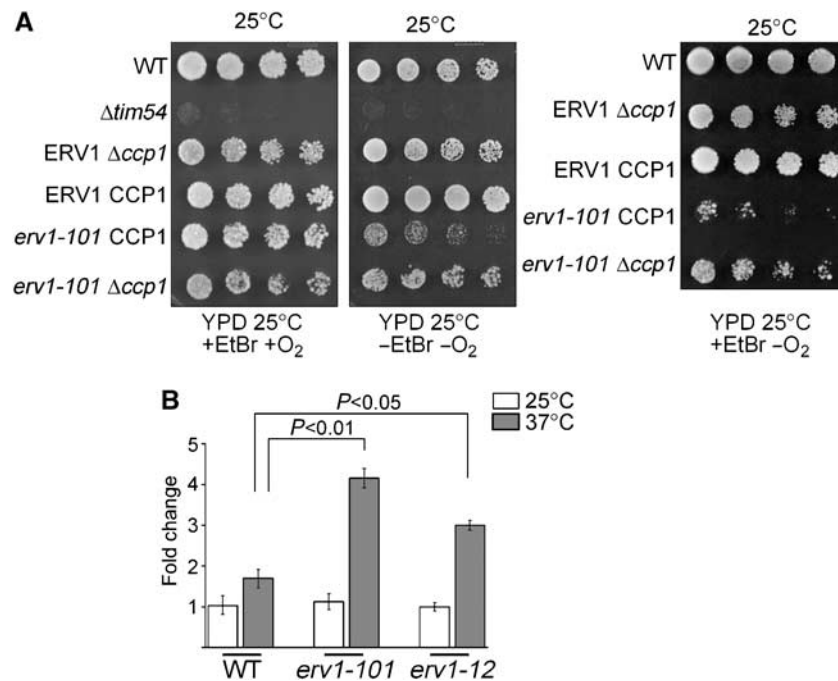
Figure 5 (**A**) A cross between *erv1-101* and Δ*ccp1* that yielded tetratype segregation was analyzed for growth as described in Figure 2D. (**B**) The *erv1* mutants accrue elevated levels of H_2O_2. Yeast cells from the parental strain (WT) and *erv1-101* and *erv1-12* (grown in YPD to mid-log phase at 25°C or shifted to 37°C for 3 h) were incubated with DCFH-DA for 3 h. H_2O_2 production of samples incubated at 25°C (white bars) and 37°C (grey bars) was measured in arbitrary fluorescence units, which are presented as fold change with the WT at 25°C being set to '1'. $n = 3$.

ERV1 for synthetic lethality at 25°C (Figure 5A). Tetrad analysis showed that strains deleted for *ccp1* in the *erv1* mutant background were viable at 25°C when the mitochondrial genome was absent. In addition, the *erv1-101* mutant grew, albeit slowly, in anaerobic conditions, similar to that in Figure 2D, regardless if *CCP1* was present. Thus, *CCP1* and *ERV1* are not synthetic lethal, indicating that *CCP1* is not strictly required for growth under the conditions investigated.

Reactions catalyzed by flavin-dependent sulfhydryl oxidases generate disulfide bonds with the reduction of O_2 to H_2O_2. We, therefore, measured H_2O_2 levels in the *erv1* mutants (Figure 5B) *in vivo* to determine if H_2O_2 levels were altered. The parental strain and *erv1-101* and *erv1-12* mutants were grown to mid-log phase and maintained at 25°C or shifted to 37°C for 3 h. H_2O_2 levels were measured using the fluorescent indicator (DCFH-DA) and fluorescence was monitored at 530 nm. H_2O_2 levels were significantly elevated in the *erv1* mutants at 37°C, supporting that Ccp1 function is impaired.

Using recombinant Ccp1 and Erv1 and oxidized cyt *c*, we measured O_2 consumption of Erv1 in the presence of excess DTT, a non-physiological electron donor, using an O_2 electrode. In the absence of Erv1, cyt *c* and Ccp1 did not consume O_2 whether alone or in combination (data not shown). When Erv1 was added alone, or in the presence of either oxidized cyt *c* or Ccp1, the rate of O_2 consumption was similar (Figure 6A; Table II). Analysis of complete oxygen electrode traces from air saturation to zero oxygen concentration allowed rates to be determined by drawing tangents to the curve for a range of oxygen concentrations. The addition of cyt *c*, however, caused a slight delay in O_2 consumption of 16 ± 0.2 s, suggesting that oxidized cyt *c* could suppress the oxygen consumption by Erv1 in presence of DTT *in vitro*.

Interestingly, previous *in vitro* studies have shown that cyt *c* is about a 100-fold better substrate than oxygen for ALR (Farrell and Thorpe, 2005). Furthermore, when Ccp1 was added in combination with oxidized cyt *c*, the rate of O_2 consumption by Erv1 was slowed by 50–60%, suggesting a synergistic interaction between cyt *c* and Ccp1 (Figure 6B; Table II; Supplementary Figure 4). As an independent measure of peroxide formation, aliquots from the above Erv1 oxidation reactions were mixed with a colorimetric reagent for the quantitation of H_2O_2. The levels of H_2O_2 decreased significantly when both cyt *c* and Ccp1 were pre-incubated with Erv1 (Figure 6C). Non-related proteins BSA and GST were used as controls to confirm the specificity of the reaction. Thus, these *in vitro* assays support the notion that Erv1 can potentially donate electrons to both O_2 and cyt *c*; however, cyt *c* is the preferred oxidant *in vitro*. The observation that the addition of both cyt *c* and Ccp1 is synergistic can be explained by the known ability of Ccp1 to oxidize cyt *c*, which would make re-oxidized cyt *c* continuously available as an electron acceptor for Erv1. Thus, Ccp1 addition 'perpetuates' the reaction by re-oxidizing the cyt *c* that is reduced by Erv1.

Ccp1 and cyt c fail to bind to heme in the erv1 mutants
Lill and co-workers have previously shown that Erv1 plays an unknown role in the maturation of cytosolic FeS clusters (Lange *et al*, 2001), thereby implying that Erv1 might have several functions. During biochemical analyses, we observed that Ccp1 migrated aberrantly in the *erv1* mutants (Figure 1B) and postulated that Erv1 might function in heme loading for Ccp1 and/or cyt *c*. We therefore tested the ability of cyt *c* and Ccp1 to bind to heme in the *erv1* mutants by investigating protease resistance and assaying for heme binding in colorless native gels (Figure 7). Typically, cyt *c* and Ccp1 are
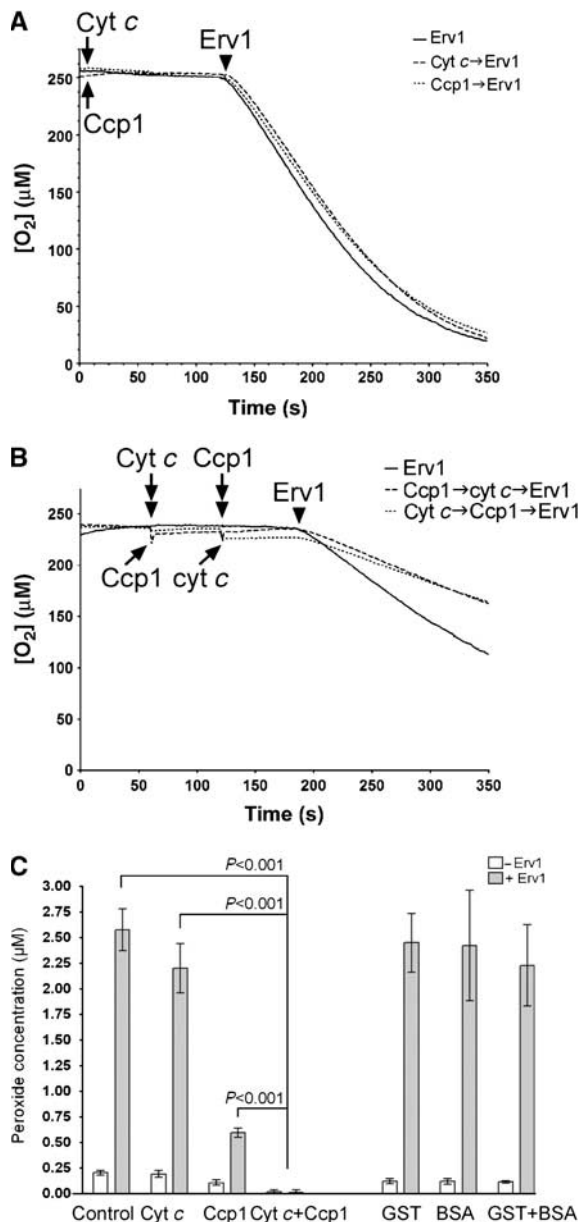
Figure 6 The Ccp1–cyt c couple competes with O₂ for Erv1-mediated oxidation of DTT. (**A**) O₂ consumption was measured in the O₂ electrode (1 ml volume) after the addition of 2 μM Erv1 (denoted with arrowhead) to air-saturated buffer containing 2 mM DTT either in the presence of 20 μM cyt c (dashed line) or 20 μM Ccp1 (dotted line) or in the absence of both cyt c and Ccp1 (solid line). (**B**) As in (A), except that all three proteins were added successively in the following order (Ccp1→cyt c→Erv1 depicted by the dashed line, cyt c→Ccp1→Erv1 depicted by the dotted line, and Erv1 alone depicted by the solid line). O₂ consumption was observed upon Erv1 addition. (**C**) As in (B), similar experiments were performed with 10 μM DTT, 1 μM Erv1, 1 μM Ccp1, and 1 μM cyt c, except that H₂O₂ concentration was measured after 30 min as described in the Supplementary data. Either cyt c or Ccp1 alone with DTT, and cyt c with Ccp1 and DTT were incubated in the absence (white bars) or presence of Erv1 (grey bars). To confirm specificity, non-related proteins BSA and GST were used as controls. Error bars indicate s.e.m. $n = 3$.

resistant to exogenous proteases, because they fold tightly around heme (Kaput et al, 1989; Claypool et al, 2006). We incubated mitochondrial lysates from the erv1-12 (Figure 7A) and erv1-101 (data not shown) mutants in the presence of

Table II O₂ consumption assays with purified components in the presence of DTT

Substrates added[a]	μM O₂ consumed/sec
cyt c	-0.001 ± 0.001
Ccp1	-0.001 ± 0.003
cyt c→Ccp1	-0.002 ± 0.003
Erv1	-0.860 ± 0.001
Erv1→cyt c	-0.763 ± 0.003
Erv1→Ccp1	-0.655 ± 0.003
cyt c→Ccp1→Erv1	-0.406 ± 0.001
Ccp1→cyt c→Erv1	-0.472 ± 0.001
cyt c→Erv1→Ccp1	-0.345 ± 0.001
Ccp1→Erv1→cyt c	-0.454 ± 0.001

[a]Substrates are listed in order of addition.

increasing concentrations of proteinase K (Figure 7B and C). As expected, protease-sensitive Kdh was degraded in the presence of proteinase K. In the erv1-12 mutants, both cyt c and Ccp1 were surprisingly protease sensitive. The erv1 mutants were then grown in media supplemented with hemin, which acts as an exogenous heme source for heme-binding proteins in the absence of heme synthesis. Upon heme supplementation, protease resistance to Ccp1 and cyt c was nearly restored, indicating that the protein's folding state was corrected by heme addition. These results indicate that heme binding may be impaired or rate-limiting for both cyt c and Ccp1 assembly in the erv1 mutants and that Erv1 may also function in heme maturation.

We adapted the staining method used for detecting heme-binding proteins in denaturing gels (Stugard et al, 1989; Grandier-Vazeille and Guerin, 1996), because Ccp1 does not bind to heme covalently. Mitochondria from the parent and erv1-12, erv1-101, Δccp1, and ccp1^H242P (Tatsuta et al, 2007) strains were solubilized in 1% digitonin and separated on colorless native gels (Figure 7D). The ccp1^H242P strain contains a mutation in the heme-binding site that renders the enzyme inactive, but is postulated to still bind heme weakly (Kaput et al, 1989). From immunoblot analysis of colorless native gels, Erv1, Ccp1, and cyt c seemed to migrate at a similar molecular weight in mitochondria that have been shifted to 37°C (indicated by the arrows). As purified cyt c does not migrate into the colorless native gel because of its very basic iso-electric point, the data of Figure 7D suggest that cyt c might be complexed with both Erv1 and Ccp1 (to form a ternary complex) at the nonpermissive temperature. In addition, the heme staining assay indicated that Ccp1 in the erv1 mutants binds to heme weakly, because it shares the same aberrant heme-binding pattern observed in Ccp1^H242P. We, therefore, propose that in addition to disulfide bond assembly and FeS cluster maturation, Erv1 may play a role in heme maturation/export in the IMS.

Erv1 does not play a role in Ccp1 processing

Ccp1 from the erv1 mutants at 37°C migrated aberrantly on SDS–PAGE gels (Figure 1B); we, therefore, inspected Ccp1 processing in detail (Supplementary Figure 5). Lysates were purified from the Δafg3 strain, which mediates the first cleavage of the Ccp1 targeting sequence, and Δpcp1, which mediates the second cleavage, as controls (Esser et al, 2002; Tatsuta et al, 2007). Ccp1 migration was investigated on an 11% SDS gel by immunoblot analysis. Ccp1 migrated slowly

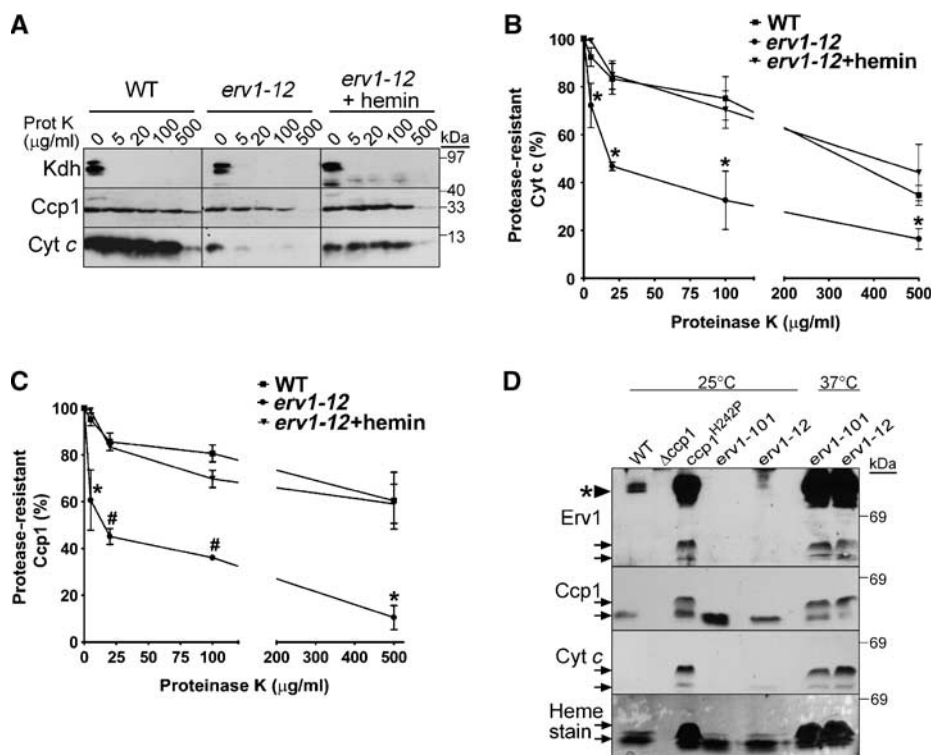**Figure 7** Heme binding in cyt *c* and Ccp1 is impaired in the *erv1* mutants. (**A**) Mitochondria were purified from the parental strain and *erv1-12* strain grown at 25°C in the presence and absence of 20 μM hemin. Subsequently, mitochondria were incubated in 0.1% Triton-X buffer with the indicated concentration of proteinase K for 30 min on ice. Proteinase K was inactivated with 1 mM PMSF followed by acid-precipitation. Samples were separated by SDS–PAGE and immunoblotted with antibodies against Kdh, Ccp1, and cyt *c*. Kdh was used as a control for protease treatment. (**B, C**) The fraction of cyt *c* (B) and Ccp1 (C) resistant to protease was quantitated with a BioRad Versadoc and the affiliated Quantity 1 software *$P < 0.01$ and #$P < 0.001$ ($n = 3$). (**D**) Mitochondria from the parental, $\Delta ccp1$, $ccp1^{H242P}$, *erv1-101*, and *erv1-12* strains grown at either 25°C or 37°C were solubilized as in Figure 2A and separated on a 6–16% Colorless Native Polyacrylamide gel. Hemoproteins were visualized after TMBZ staining. In repetitive gels, the same samples were transferred to PVDF membranes for immunoblotting with antisera against Erv1, Ccp1, and cyt *c*. Arrows indicate bands recognized by all of the above antibodies and stained by TMBZ as well, whereas the arrowhead denoted by an asterisk marks a putative Erv1 complex in WT mitochondria.

in the $\Delta afg3$ and $\Delta pcp1$ lysates because of inhibited processing. However, Ccp1 from the *erv1* mutants at both 25°C and 37°C migrated identically to Ccp1 from WT mitochondria. Erv1 most likely does not mediate Ccp1 processing; instead Ccp1 may migrate aberrantly in different gel systems (15% SDS–PAGE in Figure 1B versus 11% in Supplementary Figure 5).

Discussion

This study presents the first detailed examination of the redox behavior of Erv1, putting it into perspective with other sulfhydryl oxidases. In addition, we investigated potential pathways that might be utilized as terminal electron acceptors by Erv1.

Erv1 has three redox active centers

Using the average of the results of redox titrations carried out with either mBBr (Figure 3A) or intrinsic tryptophan fluorescence (Figure 3B) used to monitor the redox state of this dithiol/disulfide couple, the C30–C33 pair seemingly has a midpoint potential of -320 mV (at pH 7.0). DTNB analysis of the thiol content of Erv1 samples poised at defined ambient potentials, as well as non-reducing SDS–PAGE analysis of these samples, both confirm that this $E_m = -320$ mV couple involves an intermolecular disulfide and is consistent with the idea that this cysteine pair most likely mediates Erv1

dimerization *in vivo* (Hofhaus *et al*, 2003). The very low redox potential ensures that this disulfide bond is maintained in the oxidized state continuously, as it is most likely important in maintaining the catalytically active conformation of Erv1 but not involved in its redox cycle.

The E_m for the flavin component was determined to be -215 mV at pH 7.0, a value that is more negative than the $E_m = -178$ mV measured for the FAD prosthetic group of ALR at pH 7.5 (Farrell and Thorpe, 2005). As reduction of an FAD involves the uptake of two protons per FAD at all pH values below the pK_a values of the reduced FAD, one would predict pH dependence for the E_m of an FAD of -59 mV per pH unit. Thus, extrapolation suggests that the E_m value for the FAD group of ALR at pH 7.0 would be approximately -150 mV, making the difference in the E_m values for the flavins of these two related proteins strikingly different. Another difference in the properties of the Erv1 FAD, compared to this prosthetic group in related proteins, is that a small amount of semiquinone was detected during reductive titrations of both ALR and Erv2 (Farrell and Thorpe, 2005; Wang *et al*, 2007), whereas no FAD semiquinone was detected during equilibrium electrochemical titrations of Erv1. However, it is possible that an appreciable amount of Erv1 semiquinone could be formed transiently during enzyme turnover.

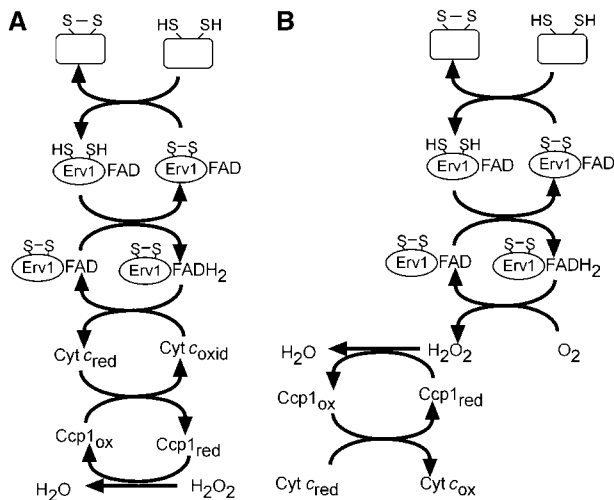The most positive redox center found in Erv1 is the redox-active, intramolecular C130–C133 pair, which has a midpoint

Figure 8 Schematic illustrating potential redox pathways with Erv1, cyt *c*, and Ccp1. See text for details.

potential of -150 mV at pH 7.0. As the most positive redox center in the molecule, it would be expected to serve as the electron sink for the protein under conditions where all three of Erv1's redox centers are allowed to come into redox equilibrium. Interestingly, the equivalent cysteine pair (C142–C145) in ALR has been proposed to be more negative than -178 mV, because this pair was not reduced during reductive titrations (Farrell and Thorpe, 2005). Considering the midpoint potentials measured in this study, the thermodynamically most favorable direction for the flow of reducing equivalents would be from the $FADH_2$ to the C130–C133 disulfide of Erv1. However, the 65 mV difference in the midpoint potentials of the two centers indicates that electron flow in the reverse direction does not face an insurmountably large thermodynamic barrier. In fact, published data from our lab and others (Farrell and Thorpe, 2005; Coppock and Thorpe, 2006; Wang *et al*, 2007) support the notion that reducing equivalents instead flow in the opposite direction (Figure 8). Furthermore, the transfer of reducing equivalents from the C130–C133 dithiol pair to FAD is likely to be kinetically favorable in that Erv1 oxidizes substrates such as Mia40 in the IMS (Terziyska *et al*, 2005). Although the midpoint potential of Mia40 is not known, we would predict that it would be more reducing than the C130–C133 dithiol pair.

Erv1 shuttles electrons to cyt *c*
Sulfhydryl oxidases, like Erv1, catalyze the formation of disulfide bonds using molecular O_2 and releasing H_2O_2. Therefore, it seemed likely that O_2 should serve as the final electron acceptor for Erv1-mediated reactions. From our study, cyt *c* is a likely candidate for a direct electron acceptor, because it partners with Erv1 *in organello* (Figure 2A) and *in vitro* as shown by the spectral perturbation assays (Figure 4B). In addition, Erv1 directly reduced cyt *c*, indicating that electrons can flow from Erv1 to cyt *c* (Figure 4C). From our genetic studies, the *erv1-101* mutant required *CYC3* for viability under anaerobic conditions. However, an obvious mechanism for the reduction of cyt *c* by the redox-active C130–C133 dithiol pair is not apparent. While this reaction would be thermodynamically favorable given the

E_m for cyt *c* is $+250$ mV and for C130–C133 pair is -150 mV, cyt *c* reduction is a one-electron reaction and dithiol oxidation to a disulfide is a two-electron reaction. As our spectral perturbation measurements indicate that there is only one high-affinity binding site for cyt *c* on Erv1, this pathway for cyt *c* reduction would require the coupling of a two-electron oxidation to a one-electron reduction. Reduction of cyt *c* by Erv1's flavin, if it were to involve a one-electron transfer involving a transiently formed FAD semiquinone seems more likely, but clearly additional experiments are required before a detailed mechanism is available.

Studies by Tokatlidis and co-workers suggest that the protein import process is linked to the electron transport chain via the connection of Erv1 with cyt *c* (Allen *et al*, 2005); however, we show that the *erv1* mutants are viable on ethidium bromide, which disrupts the electron transport chain. Therefore, additional electron acceptors must be present to reoxidize cyt *c*. Ccp1 is one logical candidate for this role and our demonstration that Ccp1 acts synergistically with cyt *c* in competing with O_2 for reduced Erv1 (Figure 6B and C) is consistent with this hypothesis. In addition, H_2O_2 levels accumulate in the *erv1* mutants at the restrictive temperature (Figure 5B). Thus, we propose that one of the Erv1 electron acceptor pathways relies on cyt *c* (Figure 8A). A large proportion of oxidized cyt *c* is available to accept electrons from Erv1 in the mitochondrion (Morgan and Wikstrom, 1991; Cortese *et al*, 1995). Reduced cyt *c* can then be re-oxidized using a variety of pathways, including the electron transport chain and Ccp1. Because cyt *c* is oxidized and reduced on the same face of the protein (Bosshard *et al*, 1986), interactions with Erv1 are most likely dynamic. This potentially dynamic interaction may allow Erv1 to use O_2 and additional acceptors. Interestingly, the yeast genome has two genes for cyt *c*, *CYC1* and *CYC7*, which are expressed under high and low O_2 concentrations, respectively (Burke *et al*, 1997). These different forms of cyt *c* may accommodate Erv1 function under different O_2 concentrations.

Ccp1 functions as a terminal electron acceptor for Erv1
Erv1 also can use O_2 as an electron acceptor, producing H_2O_2 in the IMS. We propose that Ccp1 efficiently removes accumulating H_2O_2, reducing it to water (Figure 8B). Oxidized Ccp1 in turn can be reduced and recycled by reduced cyt *c*. Our studies with the O_2 electrode suggest that Ccp1 and cyt *c* are synergistic with Erv1 and that both proposed pathways in Figure 8 may occur simultaneously. The results from colorless native gel analysis (Figure 7D) argue that Erv1, Ccp1, and cyt *c* may form a ternary complex in the *erv1* mutants at the restrictive temperature; however, this was not confirmed with other biochemical methods such as co-purification (Figure 2A and B). Subsequent studies will be required to identify additional *bonafide* Erv1 partners and substrates.

Based on our genetic studies, we also propose that an anaerobic pathway is present to recycle Erv1, because the *erv1* mutants grew in anaerobic conditions and in the absence of an electron transport chain. It may be that the cyt *c* coded by *CYC7* facilitates electron transfer under these conditions, but other unidentified acceptors may also be present. This is not unexpected because similar strategies are employed by bacteria dependent upon the aerobic/anaerobic state (Bader *et al*, 1999).

Erv1 has also been proposed to play a role in the export of FeS clusters and cellular iron homeostasis (Lange *et al*, 2001),

indicating Erv1 may have more than one function in the IMS. In our study of *erv1* mutants, cyt *c* and Ccp1 showed compromised heme binding as demonstrated by the increased sensitivity to protease. This phenotype was partially restored by the addition of exogenous hemin, suggesting that *erv1* mutants are probably heme deficient. Additionally, the *erv1* mutants showed the same aberrant heme staining pattern on colorless native gels as observed in the *ccp1*[H242P] strain. Ccp1 in the *ccp1*[H242P] strain shows reduced heme binding, because the imidazole of the specific histidine residue is involved in a pseudocovalent bond with the heme iron (Bosshard *et al*, 1986). This may be a direct effect caused by nonfunctional Erv1 or a secondary effect caused by general changes in the redox status of the IMS. At present, the details of heme export into the IMS are not clearly understood.

This study begins to dissect the different possible electron-accepting pathways for re-oxidizing reduced Erv1. Cyt *c*, which forms a high-affinity 1:1 complex with Erv1, has been shown to serve as a direct electron acceptor from reduced Erv1. Ccp1 serves a dual function, reducing the H_2O_2 generated by Erv1's reduction of O_2 and also re-oxidizing the cyt *c* reduced directly by Erv1. Additional studies, designed to elucidate these pathways in greater detail, are currently underway in our laboratories.

Materials and methods

Plasmids and strains

To generate recombinant Erv1 and Ccp1, both containing a C-terminal His$_6$ tag, the open reading frames were cloned separately into the pET28a vector (Novagen). Erv1-His$_6$ and Ccp1-His$_6$ were induced in BL21-CodonPlus (DE3)-RIL *Escherichia coli* (Stratagene) and purified under native conditions using Ni^{2+}-agarose (Qiagen) as per the manufacturer's instructions.

Standard genetic techniques were used for the yeast strains. Strains listed in this study are described in the strain table (Supplementary Table I) Temperature-sensitive (ts) *erv1* strains were generated using error-prone PCR and plasmid shuffling as described previously (Koehler *et al*, 1998). Briefly, the *erv1* mutants were cloned by *in vivo* recombination with a gapped centromeric plasmid in strain yEPL1. After plasmid shuffling to remove the WT *ERV1* plasmid, the *erv1* mutants were identified based on growth at 25°C and arrest at 37°C; the mutants were designated *erv1-101* and *erv1-12*. The Erv1-His tagged strain was constructed by subcloning *ERV1* with a 10XHis tag into pRS425, and transforming this plasmid into the yEPL1 strain for plasmid shuffling. For heme studies, yeast cells were grown in the presence of 20 μM hemin before mitochondrial isolation. The yeast strain *ccp1*[H242P] (Tatsuta *et al*, 2007) and plasmid p*ERV1*:URA32μ were kindly provided by Dr Thomas Langer and Dr Patrice Hamel, respectively.

Detailed Materials and methods for additional techniques are provided in the Supplementary data.

Supplementary data

Supplementary data are available at *The EMBO Journal* Online (http://www.embojournal.org).

References

Allen S, Balabanidou V, Sideris DP, Lisowsky T, Tokatlidis K (2005) Erv1 mediates the Mia40-dependent protein import pathway and provides a functional link to the respiratory chain by shuttling electrons to cytochrome *c*. *J Mol Biol* **353**: 937–944

Allen S, Lu H, Thornton D, Tokatlidis K (2003) Juxtaposition of the two distal 'CX3C' motifs via intrachain disulfide bonding is essential for the folding of Tim10. *J Biol Chem* **278**: 38505–38513

Bader M, Muse W, Ballou DP, Gassner C, Bardwell JC (1999) Oxidative protein folding is driven by the electron transport system. *Cell* **98**: 217–227

Bosshard HR, Davidson MW, Knaff DB, Millett F (1986) Complex formation and electron transfer between mitochondrial cytochrome *c* and flavocytochrome c_{552} from *Chromatium vinosum*. *J Biol Chem* **261**: 190–193

Boveris A (1976) Mitochondrial production of hydrogen peroxide in *Saccharomyces cerevisiae*. *Acta Physiol Lat Am* **26**: 303–309

Burke PV, Raitt DC, Allen LA, Kellogg EA, Poyton RO (1997) Effects of oxygen concentration on the expression of cytochrome *c* and cytochrome *c* oxidase genes in yeast. *J Biol Chem* **272**: 14705–14712

Chacinska A, Pfannschmidt S, Wiedemann N, Kozjak V, Sanjuan Szklarz LK, Schulze-Specking A, Truscott KN, Guiard B, Meisinger C, Pfanner N (2004) Essential role of Mia40 in import and assembly of mitochondrial intermembrane space proteins. *EMBO J* **23**: 3735–3746

Claypool SM, McCaffery JM, Koehler CM (2006) Mitochondrial mislocalization and altered assembly of a cluster of Barth syndrome mutant tafazzins. *J Cell Biol* **174**: 379–390

Coppock DL, Thorpe C (2006) Multidomain flavin-dependent sulfhydryl oxidases. *Antioxid Redox Signal* **8**: 300–311

Cortese JD, Voglino AL, Hackenbrock CR (1995) Persistence of cytochrome *c* binding to membranes at physiological mitochondrial intermembrane space ionic strength. *Biochim Biophys Acta* **1228**: 216–228

Curran SP, Leuenberger D, Oppliger W, Koehler CM (2002a) The Tim9p–Tim10p complex binds to the transmembrane domains of the ADP–ATP carrier. *EMBO J* **21**: 942–953

Curran SP, Leuenberger D, Schmidt E, Koehler CM (2002b) The role of the Tim8p–Tim13p complex in a conserved import pathway for mitochondrial polytopic inner membrane proteins. *J Cell Biol* **158**: 1017–1027

Dumont ME, Ernst JF, Sherman F (1988) Coupling of heme attachment to import of cytochrome *c* into yeast mitochondria. Studies with heme lyase-deficient mitochondria and altered apocytochromes *c*. *J Biol Chem* **263**: 15928–15937

Erman JE, Vitello LB (2002) Yeast cytochrome *c* peroxidase: mechanistic studies via protein engineering. *Biochim Biophys Acta* **1597**: 193–220

Esser K, Tursun B, Ingenhoven M, Michaelis G, Pratje E (2002) A novel two-step mechanism for removal of a mitochondrial signal sequence involves the mAAA complex and the putative rhomboid protease Pcp1. *J Mol Biol* **323**: 835–843

Farrell SR, Thorpe C (2005) Augmenter of liver regeneration: a flavin-dependent sulfhydryl oxidase with cytochrome *c* reductase activity. *Biochemistry* **44**: 1532–1541

Gabriel K, Milenkovic D, Chacinska A, Muller J, Guiard B, Pfanner N, Meisinger C (2007) Novel mitochondrial intermembrane space proteins as substrates of the MIA import pathway. *J Mol Biol* **365**: 612–620

Grandier-Vazeille X, Guerin M (1996) Separation by blue native and colorless native polyacrylamide gel electrophoresis of the oxidative phosphorylation complexes of yeast mitochondria solubilized by different detergents: specific staining of the different complexes. *Anal Biochem* **242**: 248–254

Herrmann JM, Kohl R (2007) Catch me if you can! Oxidative protein trapping in the intermembrane space of mitochondria. *J Cell Biol* **176:** 559–563

Hirasawa M, Schurmann P, Jacquot JP, Manieri W, Jacquot P, Keryer E, Hartman FC, Knaff DB (1999) Oxidation-reduction properties of chloroplast thioredoxins, ferredoxin:thioredoxin reductase, and thioredoxin f-regulated enzymes. *Biochemistry* **38:** 5200–5205

Hofhaus G, Lee JE, Tews I, Rosenberg B, Lisowsky T (2003) The N-terminal cysteine pair of yeast sulfhydryl oxidase Erv1p is essential for *in vivo* activity and interacts with the primary redox centre. *Eur J Biochem* **270:** 1528–1535

Hoober KL, Joneja B, White HB, Thorpe C (1996) A sulfhydryl oxidase from chicken egg white. *J Biol Chem* **271:** 30510–30516

Kadokura H, Katzen F, Beckwith J (2003) Protein disulfide bond formation in prokaryotes. *Annu Rev Biochem* **72:** 111–135

Kaput J, Brandriss MC, Prussak-Wieckowska T (1989) *In vitro* import of cytochrome c peroxidase into the intermembrane space: release of the processed form by intact mitochondria. *J Cell Biol* **109:** 101–112

Koehler CM (2004) The small Tim proteins and the twin Cx3C motif. *Trends Biochem Sci* **29:** 1–4

Koehler CM, Beverly KN, Leverich EP (2006) Redox pathways of the mitochondrion. *Antioxid Redox Signal* **8:** 813–822

Koehler CM, Jarosch E, Tokatlidis K, Schmid K, Schweyen RJ, Schatz G (1998) Import of mitochondrial carriers mediated by essential proteins of the intermembrane space. *Science* **279:** 369–373

Krimm I, Lemaire S, Ruelland E, Miginiac-Maslow M, Jaquot JP, Hirasawa M, Knaff DB, Lancelin JM (1998) The single mutation Trp35→Ala in the 35-40 redox site of *Chlamydomonas reinhardtii* thioredoxin *h* affects its biochemical activity and the pH dependence of C36-C39 1H-13C NMR. *Eur J Biochem* **255:** 185–195

Lange H, Lisowsky T, Gerber J, Muhlenhoff U, Kispal G, Lill R (2001) An essential function of the mitochondrial sulfhydryl oxidase Erv1p/ALR in the maturation of cytosolic Fe/S proteins. *EMBO Rep* **2:** 715–720

Lee J, Hofhaus G, Lisowsky T (2000) Erv1p from *Saccharomyces cerevisiae* is a FAD-linked sulfhydryl oxidase. *FEBS Lett* **477:** 62–66

Leuenberger D, Curran SP, Wong D, Koehler CM (2003) The role of Tim9p in the assembly of the TIM22 import complexes. *Traffic* **4:** 144–152

Lisowsky T (1992) Dual function of a new nuclear gene for oxidative phosphorylation and vegetative growth in yeast. *Mol Gen Genet* **232:** 58–64

Lu H, Golovanov AP, Alcock F, Grossmann JG, Allen S, Lian LY, Tokatlidis K (2004) The structural basis of the TIM10 chaperone assembly. *J Biol Chem* **279:** 18959–18966

Mesecke N, Terziyska N, Kozany C, Baumann F, Neupert W, Hell K, Herrmann JM (2005) A disulfide relay system in the intermembrane space of mitochondria that mediates protein import. *Cell* **121:** 1059–1069

Morgan JE, Wikstrom M (1991) Steady-state redox behavior of cytochrome c, cytochrome a, and CuA of cytochrome c oxidase in intact rat liver mitochondria. *Biochemistry* **30:** 948–958

Ondrias MR, Carson SD, Hirasawa M, Knaff DB (1985) Characterization of the siroheme active site in spinach nitrite reductase by resonance Raman spectroscopy. *Biochim Biophys Acta* **830:** 159–163

Rissler M, Wiedemann N, Pfannschmidt S, Gabriel K, Guiard B, Pfanner N, Chacinska A (2005) The essential mitochondrial protein Erv1 cooperates with Mia40 in biogenesis of intermembrane space proteins. *J Mol Biol* **353:** 485–492

Senkevich TG, White CL, Koonin EV, Moss B (2002) Complete pathway for protein disulfide bond formation encoded by poxviruses. *Proc Natl Acad Sci USA* **99:** 6667–6672

Sevier CS, Cuozzo JW, Vala A, Aslund F, Kaiser CA (2001) A flavoprotein oxidase defines a new endoplasmic reticulum pathway for biosynthetic disulphide bond formation. *Nat Cell Biol* **3:** 874–882

Stugard CE, Daskaleros PA, Payne SM (1989) A 101-kilodalton heme-binding protein associated with congo red binding and virulence of *Shigella flexneri* and enteroinvasive *Escherichia coli* strains. *Infect Immun* **57:** 3534–3539

Tatsuta T, Augustin S, Nolden M, Friedrichs B, Langer T (2007) m-AAA protease-driven membrane dislocation allows intramembrane cleavage by rhomboid in mitochondria. *EMBO J* **26:** 325–335

Terziyska N, Lutz T, Kozany C, Mokranjac D, Mesecke N, Neupert W, Herrmann JM, Hell K (2005) Mia40, a novel factor for protein import into the intermembrane space of mitochondria is able to bind metal ions. *FEBS Lett* **579:** 179–184

Wallace CJ (1984) The effect of complete or specific partial acetimidylation on the biological properties of cytochrome c and cytochrome c-T. *Biochem J* **217:** 595–599

Wang W, Winther JR, Thorpe C (2007) Erv2p: characterization of the redox behavior of a yeast sulfhydryl oxidase. *Biochemistry* **46:** 3246–3254

Webb CT, Gorman MA, Lazarou M, Ryan MT, Gulbis JM (2006) Crystal structure of the mitochondrial chaperone TIM9.10 reveals a six-bladed alpha-propeller. *Mol Cell* **21:** 123–133

Wiedemann N, Pfanner N, Chacinska A (2006) Chaperoning through the mitochondrial intermembrane space. *Mol Cell* **21:** 145–148